Title

Phase stability and mechanical properties of novel high entropy transition metal carbides

Authors

Harrington, Tyler J
Gild, Joshua
Sarker, Pranab
et al.

Publication Date

2019-03-01

DOI

10.1016/j.actamat.2018.12.054

Peer reviewed

Acta Materialia 166 (2019) 271–280

Contents lists available at ScienceDirect

Acta Materialia

journal homepage: www.elsevier.com/locate/actamat

Full length article

Phase stability and mechanical properties of novel high entropy transition metal carbides

Tyler J. Harrington [a, b], Joshua Gild [b], Pranab Sarker [c], Cormac Toher [c], Christina M. Rost [d], Olivia F. Dippo [b], Cameron McElfresh [a], Kevin Kaufmann [a], Eduardo Marin [a], Lucas Borowski [a], Patrick E. Hopkins [d], Jian Luo [a, b], Stefano Curtarolo [e], Donald W. Brenner [f], Kenneth S. Vecchio [a, b, *]

[a] Department of NanoEngineering, University of California, San Diego, La Jolla, CA, 92093, USA
[b] Materials Science and Engineering Program, University of California, San Diego, La Jolla, CA, 92093, USA
[c] Department of Mechanical Engineering and Materials Science, Duke University, Durham, NC, 27708, USA
[d] Department of Mechanical and Aerospace Engineering, University of Virginia, Charlottesville, VA, 22904, USA
[e] Materials Science, Electrical Engineering, Physics and Chemistry, Duke University, Durham, NC, 27708, USA
[f] Department of Materials Science and Engineering, North Carolina State University, Raleigh, NC, 27695, USA

ARTICLE INFO

Article history:
Received 24 August 2018
Received in revised form
28 December 2018
Accepted 28 December 2018
Available online 31 December 2018

Keywords:
Carbides
High-entropy alloys
Entropy-stabilized
Multicomponent
Hardness

ABSTRACT

Twelve different equiatomic five-metal carbides of group IVB, VB, and VIB refractory transition metals are synthesized via high-energy ball milling and spark plasma sintering. Implementation of a newly developed *ab initio* entropy descriptor aids in selection of candidate compositions for synthesis of high entropy and entropy stabilized carbides. Phase formation and composition uniformity are analyzed via XRD, EDS, S/TEM-EDS, and EXAFS. Nine of the twelve candidates form true single-phase materials with the rocksalt (B1) structure when sintered at 2473 K and can therefore be investigated as high entropy carbides (HECs). The composition $(V_{0.2}Nb_{0.2}Ta_{0.2}Mo_{0.2}W_{0.2})C$ is presented as a likely candidate for further investigation as an entropy stabilized carbide. Seven of the carbides are examined for mechanical properties via nanoindentation. The HECs show significantly enhanced hardness when compared to a rule of mixtures average of the constituent binary carbides and to the highest hardness of the binary constituents. The mechanical properties are correlated to the electronic structure of the solid solutions, offering a future route to tunability of the mechanical properties of carbide ceramics via exploration of a new complex composition space.

1. Introduction

Ultra-high temperature materials are generally defined as materials with melting temperatures ≥3300 K - a quality that is currently limited to a list of about 15 elements or compounds [1,2]. Of these, the carbides, nitrides, oxides, and borides comprise a class of materials called ultra-high temperature ceramics (UHTCs). Recently, driven by the increasingly more demanding operating conditions in structural applications, such as next generation nuclear reactors, rocket nozzles, and hypersonic vehicle leading edges, there has been a resurgence in the research and development of UHTCs. Owing to their high hardness, good corrosion resistance, and high melting temperature, the carbides of group IVB, VB, and VIB transition metals are promising candidates for the aforementioned applications [1,3,4]. Of the short list of the known UHTCs, tantalum carbide and hafnium carbide have two of the highest melting temperatures of any known materials with $T_m = 4041$ K and $T_m = 4232$ K, respectively; however, they are prone to oxidation at intermediate temperatures [1]. The diborides of Hf and Zr are therefore generally considered as the state of the art in UHTCs when operating in oxidizing environments, even though they melt at lower temperatures than the carbides [1]. As application demands increase, the short list of current UHTCs cannot fulfill all the necessary requirements and new material composition spaces must be explored. In this regard, ceramics development has begun to follow metallurgy in the investigation of high entropy systems.

* Corresponding author. Department of NanoEngineering, University of California, San Diego, La Jolla, CA, 92093, USA.
E-mail address: kvecchio@eng.ucsd.edu (K.S. Vecchio).

https://doi.org/10.1016/j.actamat.2018.12.054
1359-6454/

The newly developed field of high entropy alloys (HEAs) has garnered much research interest in recent years. In the original theory of HEAs, the high configurational entropy of chemically complex solid solution phases stabilizes them into a single crystalline phase against the formation of the thermodynamically competing intermetallics. According to this theory, when the constituent elements are present in equiatomic amounts in a single phase, the maximum molar configurational entropy of $S = R\ lnN$ is obtained, where R is the gas constant, 8.314 J mol^{-1} K^{-1}, and N is the number of components [5,6]. It is somewhat generally accepted that this molar configurational entropy becomes significant when there are five or more components, which gives $S \geq 1.61R$ [7]. Thus, HEA compositions typically comprise five or more chemical species mixed in equimolar (or close to equimolar) concentrations. It should be noted, however, that there remains significant debate over the term "high entropy alloy" regarding the actual role that entropy plays in the stability of the system, as opposed to simply being higher than systems with fewer components [8]. For instance, a five-component equiatomic system that displays a single-phase is not necessarily "entropy stabilized" (i.e., it can be enthalpically stable as well). Further, the entropy value of *1.61R* for a five-component system implies that all the elements are present in an approximately random solid solution phase that is mixed on a first nearest neighbor scale, which means that any material that is not homogeneous or that forms multiple phases is not a HEA; thus the terms multi-principle element alloy (MPEA) and complex concentrated alloy (CCA) have been recently applied to these systems [7,9]. For this work, we deem it important to differentiate between a high entropy material and an entropy stabilized material. A high entropy material implies only that the configurational entropy is significant, meaning that the elements are present in a random solid solution phase. An entropy stabilized material implies that the solid solution phase only exists due to the high configurational entropy (i.e. the molar heat of mixing is positive). Regardless of the "role of entropy" debate, the exploration of the high entropy material space is growing rapidly and significant developments are being made, which are quickly advancing the understanding of these materials on a fundamental level and accelerating their development for applications as structural materials [7,8]. To date, a myriad of HEA compositions have been synthesized and studied, and many have demonstrated exceptional mechanical and physical properties including high hardness and strength, good corrosion resistance, and high-temperature stability [6,7,10–14]. The work has also extended into the field of ceramics, where studies of oxides, carbides, borides, and nitrides are beginning to show promise for applications such as ultra-high temperature structural materials, extreme environments, and electronics [15–18].

The first bulk, crystalline, entropy stabilized ceramic $(Co_{0.2}Cu_{0.2}Mg_{0.2}Ni_{0.2}Zn_{0.2})O$, was fabricated by Rost et al. [16], illustrating the high temperature entropic stabilization as it required quenching from sufficiently high temperatures for a single phase to occur, and the transformation was endothermic on heating. This study also marks one of the first and only works to present a systematic investigation of the role that entropy plays in forcing the formation of a solid solution [19]. Thus, it provides valuable insight for resolution of the aforementioned "role of entropy" debate. Since the original work, the $(Co_{0.2}Cu_{0.2}Mg_{0.2}Ni_{0.2}Zn_{0.2})O$ system and those based on it $(Mg_{0.2}Co_{0.2}Ni_{0.2}Cu_{0.2}Zn_{0.2})_{1-x-y}Ga_yA_xO$ (where A = Li, Na, or K), have demonstrated colossal dielectric constants and room temperature lithium superionic conductivity [17,18]. Recently, in the field of UHTCs, Gild et al. [20] demonstrated successful fabrication of several crystalline, stoichiometric, high entropy diborides of group IVB, VB, and VIB refractory transition metals. The diborides showed a single hexagonal phase, which consisted of alternating layers of metal and boron nets. There has also been investigation into a variety of carbide and nitride films, which exhibit superior hardness, wear resistance and oxidation resistance compared to individual constituents [21–27]. The majority of these nitride and carbide films, while exhibiting exceptional properties, are far from the equiatomic compositions that optimize entropic stabilization and often possess an amorphous structure [7]. Yeh et al. [6] reported fabrication of a single phase bulk $(Cr_{0.2}Nb_{0.2}Ti_{0.2}V_{0.2}W_{0.2})C$ high entropy carbide via mechanical alloying and solid-state sintering, but little information is given on the properties of the material. The present authors [28] have previously developed and utilized an *ab initio* entropy descriptor to synthesize nine different five-metal carbides, six of which formed single-phase high entropy materials that demonstrated high hardness values. Recent work done by Castle et al. [29,30], demonstrated that the four component carbides $(Hf_{0.25}Ta_{0.25}Zr_{0.25}Ti_{0.25})C$ and $(Hf_{0.25}Ta_{0.25}Zr_{0.25}Nb_{0.25})C$ could be fabricated in bulk, although $(Hf_{0.25}Ta_{0.25}Zr_{0.25}Nb_{0.25})C$ more easily formed a single phase. The four component carbides demonstrated significant hardness enhancements over the expected values from rule of mixtures [29]. The work of Dusza et al. [30] showed that the $(Hf_{0.25}Ta_{0.25}Zr_{0.25}Nb_{0.25})C$ material was single phase with no detectable segregation at the micro/nanoscale level. Following the work of the present authors [28,31], the bulk five component carbide $(Hf_{0.2}Nb_{0.2}Ta_{0.2}Ti_{0.2}Zr_{0.2})C$ was fabricated by Yan et al. [32], which demonstrated low thermal conductivity and a high elastic modulus and hardness.

Here we present a systematic study of phase stability and mechanical properties in twelve bulk, equiatomic, five-metal high entropy carbides, of which eleven have never been reported. Specifically, introduction of elements from group VIB, none of which demonstrate cubic monocarbides at room temperature, allows for insight into the role of entropy in the stability of the single phase. Phase purity is examined through XRD, EDS, S/TEM, and EXAFS. Mechanical properties are presented in terms of hardness and modulus measured from nanoindentation testing and compared with rule-of-mixtures predictions based on the five constituent binary carbides as well as their relationship to electronic structure through the valence electron concentration (VEC). The study of a range of compositions spanning group IVB, VB, and VIB transition metals leads to a series of materials with different electronic structures, which allows for analysis of trends relating mechanical properties to electronic structure that can be valuable in future materials design.

2. Methods

2.1. Predicting high entropy compositions

An *ab initio* technique for determining the effective role of entropy was employed to identify compositions with a high or low propensity to form a single phase. A thorough discussion of the technique by the current authors is presented in Ref. [28] and is outside of the scope of this study, which focuses primarily on the experimental synthesis and characterization of high entropy carbides. In short, the model employs an entropy descriptor, which allows for the determination of an Entropy Forming Ability (EFA) for each material composition. To calculate the EFA, a set of 49 configurations is generated using the partial occupation (POCC) module [33] of the AFLOW (Automatic FLOW) framework [34]. The energy distributions of these sets of configurations are calculated using density functional theory as implemented in the VASP package [35], with the Perdew, Burke, Ernzerhof (PBE) parameterization of the generalized gradient approximations (GGA) exchange-correlation functional [36], and the AFLOW standard settings [37]. A narrow distribution indicates a low energy cost to introduce metastable configurations (and thus disorder) into the material, whereas a broad distribution implies a high energy barrier to add configurations. The EFA descriptor is inversely proportional to the width of the energy

distribution, so that a high EFA value corresponds to a composition that should easily form a single phase.

2.2. Synthesis and sintering

For each of the candidate compositions listed in Table 1, starting powders of each of the individual carbide compounds (TiC, ZrC, HfC, $VC_{0.88}$, NbC, TaC, Mo_2C, W_2C) (Alfa Aesar, >99.5% purity, −325mesh) were weighed out in batches of 50 g and hand mixed. Following hand mixing, the powders were high energy ball milled (HEBM) in a Spex 8000D shaker pot high energy ball mill (SpexCertPrep, NJ, USA) using tungsten carbide lined stainless steel jars and 10 mm tungsten carbide milling media for 2 h in 12 g batches with 0.1 g stearic acid as lubricant. The milling was performed in 30-min segments with 10-min cool-off periods to minimize overheating and oxide formation; all milling was performed in an argon atmosphere. The milled powders were consolidated in 12 g batches via spark plasma sintering (SPS) at 2473 K under a uniaxial load of 30 MPa for 10 min, into 20 mm pellets using a Thermal Technologies 3000 series SPS (Thermal Technologies, CA, USA). The entire sintering process was carried out in a vacuum environment at an initial value of less than 20 mTorr; final sintered pellets measured approximately 4 mm in thickness. A heating rate of 100 K/min was used throughout the entire ramp to 2473 K for each SPS run, and samples were left to cool to room temperature in argon following the 10-min dwell at the sintering temperature. All SPS steps were carried out in graphite die and plunger sets lined with graphite foil.

2.3. X-ray diffraction and electron microscopy

XRD was done on a Rigaku Miniflex diffractometer at 30 kV and 15 mA over a 2θ range of 20°−120° with 0.02° steps. SEM and EDS analyses were conducted on a Thermo Scientific Apreo electron microscope at an accelerating voltage of 20 kV. TEM sample preparation was carried out on a Thermo Scientific Scios Dual Beam FIB. S/TEM characterization was performed on a Thermo Scientific Talos S/TEM at an accelerating voltage of 200 kV.

2.4. Extended X-ray absorption fine structure

The extended x-ray absorption fine structure (EXAFS) data for V, Nb, Mo, and W was collected on the APS beamline 12-BM at Argonne National Laboratory (Lemont, IL). Tantalum was not scanned as the tantalum L absorption edges (Ta_{L1} = 11,682 eV, Ta_{L2} = 11,136 eV, Ta_{L3} = 9881 eV) lie too close to the tungsten L-edges (W_{L1} = 12,100 eV, W_{L2} = 11,544 eV, W_{L3} = 10,207 eV), making the EXAFS region for Ta inaccessible when W is also within a sample composition. The V data was collected using the vanadium K-edge at 5465 eV, molybdenum using the K-edge at 20,000 eV, niobium using the K-edge at 18,986 eV and tungsten using the L3-edge at 10,207 eV [38]. To reduce noise, each absorber was scanned a minimum of eight runs, and the reported data is the average after 'glitch' removal and background fitting. Initial raw data processing was carried out in the Athena software package [38]; data fitting to the theoretical model was conducted using Artemis [38].

2.5. Hardness testing

Hardness and modulus testing was conducted via nano-indentation on a KLA-tencor G200 Nanoindenter (KLA-tencor, CA, USA). Hardness measurements were performed according to ISO 14577 under a maximum load of 300 mN. In order to produce more statistically relevant data from the nanoindentation measurements, the KLA-tencor Express Test software module was employed. This testing method allows for modulus and hardness measurements at a rate of approx. 1 per second, thereby enabling very large datasets to be generated. For analysis of indentation size effects (ISE), which are known to be present in B1 transition metal carbides [39], an investigation of the hardness of a 99% dense sample of composition $(Ti_{0.2}Zr_{0.2}Hf_{0.2}Nb_{0.2}Ta_{0.2})C$ was done under different loading conditions. The results of the load and indentation depth dependence of the hardness measurements is given in Supplementary Fig. 1. The hardness exhibits increased values for measurements made with a max load under 50 mN (resulting indentation depth of 326 nm). A load over 50 mN leads to indents large enough to be free of indentation size effects. Indents above 300 mN show significant scatter due to crack formation and therefore cannot be used to calculate the modulus and hardness according to the standard methods of Oliver and Pharr [40]. A load of 300 mN was selected for testing of the carbide materials in this study. Nanoindentation was done on each of the binary carbides synthesized in the same manner as the HECs in this study for generation of rule of mixture moduli and hardness. Tabulated values for each of the binaries is included in Supplementary Table 1. Elastic and hardness data for rocksalt structured MoC were taken from theoretical treatments presented in Ref. [41], modulus data for rocksalt WC from calculated values in Ref. [42], and hardness for rocksalt WC from experimental values in Refs. [43,44].

2.6. Carbon combustion analysis

Analysis of the carbon content in each of four samples: $(Ti_{0.2}Hf_{0.2}V_{0.2}Nb_{0.2}Ta_{0.2})C$, $(Ti_{0.2}V_{0.2}Nb_{0.2}Ta_{0.2}W_{0.2})C$, $(Ti_{0.2}Zr_{0.2}Hf_{0.2}Ta_{0.2}W_{0.2})C$, and $(Ti_{0.2}Hf_{0.2}Nb_{0.2}Ta_{0.2}W_{0.2})C$ was done on a Perkin Elmer 2400 Series II CHNS/O Analyzer with a combustion time of 30 s

Table 1
List of compositions studied, their calculated entropy forming ability, determination of phase composition following experimental synthesis, and lattice parameter from XRD measurements. If multiple phases were present, reported lattice parameter corresponds to the highest intensity cubic phase.

Composition	EFA	Phase Composition	Secondary Phase	Lattice Parameter, a, (Å)
$(Ti_{0.2}Zr_{0.2}Hf_{0.2}Nb_{0.2}Ta_{0.2})C$	100	Single Phase	–	4.51(8)
$(Ti_{0.2}Hf_{0.2}V_{0.2}Nb_{0.2}Ta_{0.2})C$	100	Single Phase	–	4.42(1)
$(Ti_{0.2}V_{0.2}Nb_{0.2}Ta_{0.2}W_{0.2})C$	77	Single Phase	–	4.36(2)
$(Ti_{0.2}Zr_{0.2}Hf_{0.2}Ta_{0.2}W_{0.2})C$	50	Single Phase	–	4.48(7)
$(Ti_{0.2}Hf_{0.2}Nb_{0.2}Ta_{0.2}W_{0.2})C$	67	Single Phase	–	4.44(2)
$(Ti_{0.2}V_{0.2}Nb_{0.2}Ta_{0.2}Mo_{0.2})C$	100	Single Phase	–	4.36(1)
$(Ti_{0.2}Zr_{0.2}Hf_{0.2}Ta_{0.2}Mo_{0.2})C$	63	Single Phase	–	4.49(4)
$(Ti_{0.2}Hf_{0.2}Nb_{0.2}Ta_{0.2}Mo_{0.2})C$	83	Single Phase	–	4.44(3)
$(V_{0.2}Nb_{0.2}Ta_{0.2}Mo_{0.2}W_{0.2})C$	125	Single Phase	–	4.34(0)
$(Zr_{0.2}Hf_{0.2}Ta_{0.2}Mo_{0.2}W_{0.2})C$	45	Multiple Phases	$(Mo_xW_y)C$ (orth)	4.51(6)
$(Ti_{0.2}Zr_{0.2}Hf_{0.2}Mo_{0.2}W_{0.2})C$	38	Multiple Phases	$(Mo_xW_y)C$ (rs)	4.45(9)
$(Zr_{0.2}Hf_{0.2}V_{0.2}Mo_{0.2}W_{0.2})C$	37	Multiple Phases	$(Mo_xW_y)C$ (rs)	4.52(6)

at 975 °C. Prior to testing, each sample was hand ground and sifted to ≤45 μm powder, tests were run in 5 mg powder batches and the given values are an average of eight runs per sample. A $VC_{0.88}$ standard was run four times between each sample composition. The results are presented in Supplementary Table 2.

3. Results

3.1. Phase formation and EFA predictions

The compositions listed in Table 1 are given along with their calculated EFA values. Compositions with an EFA ≥50 are shown to form phase pure high entropy ceramics, while the three compositions with EFA ≤45 exhibit multiple phases after sintering at 2473 K, suggesting that the cutoff for single phase formation for five component carbides at 2473 K lies between EFA values of 45 and 50.

3.2. Structure determination

Initial determination of phase purity is carried out through X-ray diffraction (XRD) analysis. An example of a detailed investigation of phase progression in a sample of composition $(Ti_{0.2}Hf_{0.2}V_{0.2}Nb_{0.2}Ta_{0.2})C$ follows. This sample composition is used as the example for analysis in XRD, SEM, and S/TEM-EDS throughout. All other compositions were analyzed in a similar manner with results located in the Supplementary Information. The X-ray diffraction patterns of a specimen processed via hand mixing, HEBM, and SPS, collected after each processing step (i.e. hand mixed powder, high energy ball milled powder, and spark plasma sintered pellet) are shown in Fig. 1a. Five distinct cubic phases that correlate to the individual precursor powders are observed in the hand mixed powder specimen in Fig. 1b. After high energy ball milling, similar but broader peaks are observed, which can be attributed to the particle size reduction and mechanical alloying resulting from the milling. After spark plasma sintering, only the peaks from a single rocksalt phase are observed, indicating that the system has progressed toward a solid solution with a uniform lattice parameter. The final diffraction pattern is representative of a homogeneous single phase, to the extent that this can be determined in a laboratory diffractometer. The reflections are: (a) narrow in 2-theta (2θ) space, (b) demonstrate clear $K\alpha_2$ splitting in higher order peaks, and (c) free of shoulders, reinforcing the conclusion of a chemically homogeneous structure with a single lattice parameter. The relative intensities for the final patterns of each single-phase carbide match well with the structure factor calculations for a fully mixed rocksalt phase. Reitveld refinement (Supplementary Fig. 2) shows a single lattice parameter of 4.42(1) Å with a χ^2 of 3.3, indicating a good degree of fitting to the calculated, chemically mixed phase.

XRD patterns for each of the nine single phase carbide compositions are shown in Fig. 2a, and for the three multiple phase compositions in Fig. 2b. The compositions that contain only group IVB and VB transition metals each demonstrate a single phase following sintering at 2473 K. Similarly, materials that contain four species from groups IVB and VB and a single group VIB show only a cubic phase. Three of the four compositions that contain three group IVB and VB and two group VIB (i.e. both W and Mo) show multiple phases, however, of particular interest is $(V_{0.2}Nb_{0.2}Ta_{0.2}Mo_{0.2}W_{0.2})C$, which shows a single phase despite having both Mo and W in equiatomic amounts. The second phase present in each of the multiple phase compositions is a Mo and W rich phase. In $(Zr_{0.2}Hf_{0.2}Ta_{0.2}Mo_{0.2}W_{0.2})C$, this second phase is a hexagonal $(Mo_xW_y)C$ phase, while $(Ti_{0.2}Zr_{0.2}Hf_{0.2}Mo_{0.2}W_{0.2})C$ exhibits the primary mixed rocksalt phase and two secondary cubic phases, and $(Zr_{0.2}Hf_{0.2}V_{0.2}Mo_{0.2}W_{0.2})C$ exhibits the primary mixed rocksalt and a single secondary cubic phase. It should be noted that the secondary phase present in the three samples are distinct and not representative of the hexagonal WC or orthorhombic Mo_2C powder.

3.3. Determining homogeneity - microstructure and S/TEM

Following structure determination in XRD, microscale homogeneity must be determined via SEM microstructural imaging.

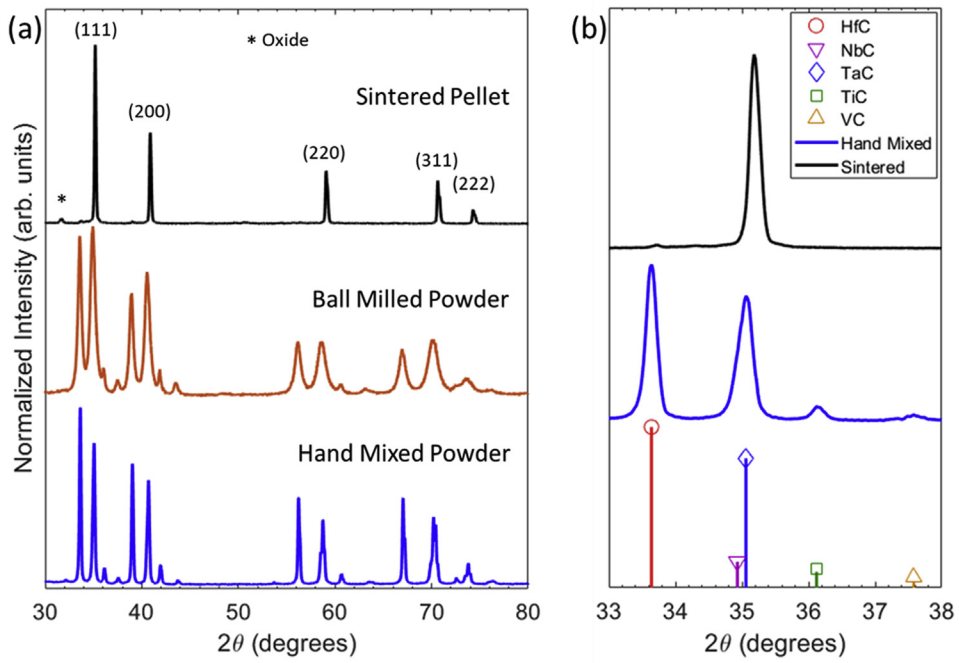

Fig. 1. X-ray diffraction patterns for the example composition $(Ti_{0.2}Hf_{0.2}V_{0.2}Nb_{0.2}Ta_{0.2})C$, through (a) each processing step: hand mixed, ball milled, and sintered demonstrating the progression into a single phase rocksalt material (lattice parameter: $a = 4.42$ Å; space group: $Fm\bar{3}m$, #225; Pearson Symbol: cF8) and (b) high magnification of the 111 peak of each of the hand mixed precursor powders and sintered product showing the final carbide with the approximate average lattice parameter of the constituents.

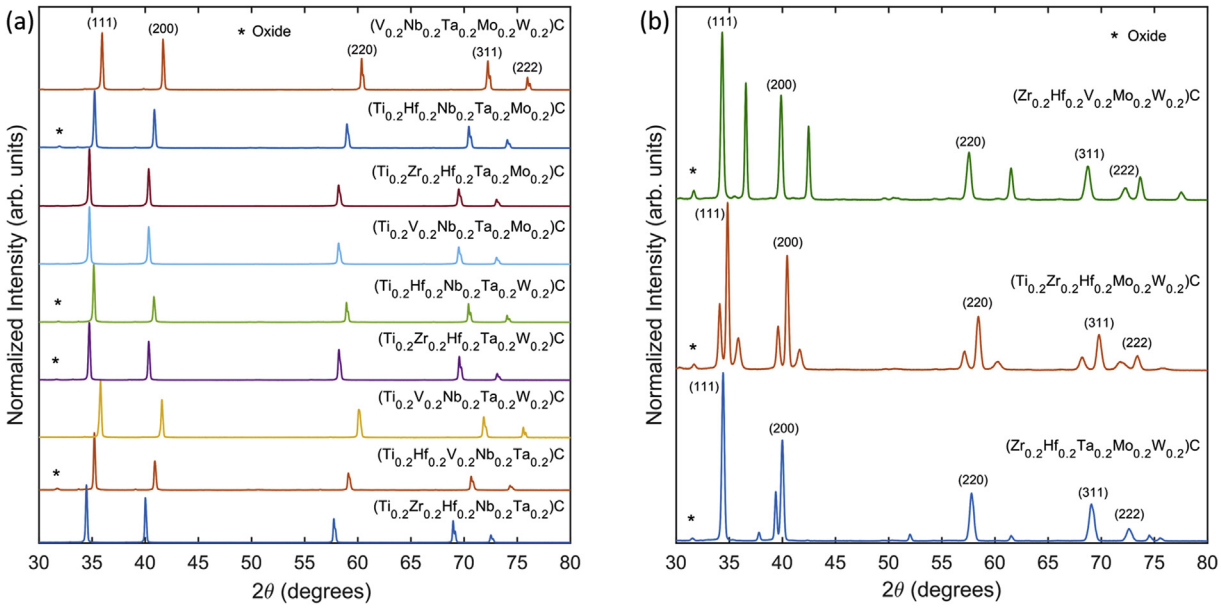

Fig. 2. X-ray diffraction patterns for (a) nine single phase compositions and (b) three multi-phase compositions. Note that the secondary (and tertiary) phases that form in the multi-phase specimens are different in each of the three compositions.

Example SEM micrographs of the example single-phase $(Ti_{0.2}Hf_{0.2}V_{0.2}Nb_{0.2}Ta_{0.2})C$ and a multi-phase $(Zr_{0.2}Hf_{0.2}Ta_{0.2}Mo_{0.2}W_{0.2})C$ sample are given in Fig. 3. Microstructure images for all twelve compositions are presented in Supplementary Fig. 3. The microstructure of the multi-phase sample shows clear grain boundary phase precipitation, while the single-phase sample demonstrates only orientation contrast and no indications of secondary phases, grain boundary or otherwise, supporting the conclusion that the rocksalt phase is mixed and homogeneous.

For nano/atomic level microstructure information, example TEM and STEM-EDS for composition $(Ti_{0.2}Hf_{0.2}V_{0.2}Nb_{0.2}Ta_{0.2})C$ is given in Fig. 4. The selected area electron diffraction (SAED) pattern for $(Ti_{0.2}Hf_{0.2}V_{0.2}Nb_{0.2}Ta_{0.2})C$ shows no signs of ordering and no additional spots, indicative of a secondary phase. The STEM-EDS exhibits no indication of elemental clustering or phase segregation. While none of the individual techniques fully prove the existence of a fully mixed single-phase material, the combination of XRD with STEM-EDS and TEM strongly supports that a true high entropy phase-pure material is formed in both cases.

3.4. Determining homogeneity — EXAFS

For entropy to be a significant contributing factor to the stability of the disordered phase, the structure must be an approximately ideally mixed and disordered, chemically homogeneous solid solution. To prove this, it must be demonstrated that only a single crystal structure exists, and that it is homogeneous on any length scale. XRD probes the d-spacing of crystals on a sample global scale, but in complex systems it offers little information about the local chemical distribution. EDS probes the chemical distribution, but it does so on a micrometer length scale when carried out in a SEM environment. S/TEM and STEM-EDS studies test the chemical distribution on the angstrom length scale; however, only a very small amount of the sample can be studied, and therefore these results may not always be representative of the bulk sample. To determine the angstrom scale local environment of each element globally in the sample, EXAFS is the ideal characterization technique.

The results from an EXAFS study of composition $(V_{0.2}Nb_{0.2}Ta_{0.2}Mo_{0.2}W_{0.2})C$ are presented in Fig. 5. The $k^2\chi I$ for each of the V, Nb, and Mo absorbers looks very similar, indicating that each of the metals has similar local surroundings [16]. Results for W and Ta are not given due to the aforementioned issues with absorption edge overlap.

Given the complex nature of HECs, verification of the local structure from measured EXAFS data relies on fitting to a theoretical structure model [45]. For a theoretical model of a disordered material, the degeneracy of the scattering paths can be used to simulate the random occupancy. In the EXAFS of a rocksalt carbide,

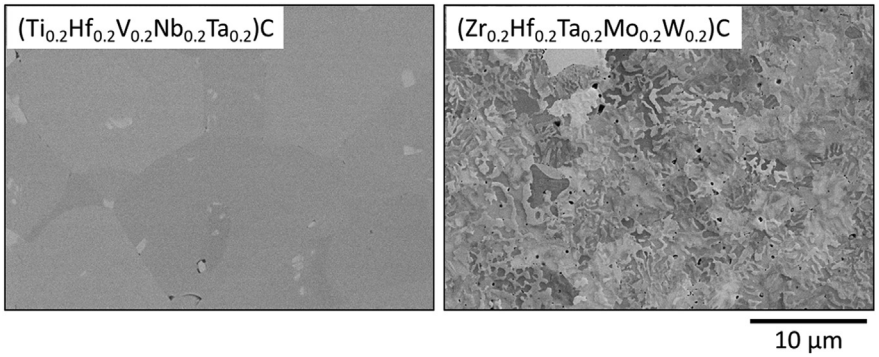

Fig. 3. Backscattered electron micrographs from (left) a single-phase specimen of composition $(Ti_{0.2}Hf_{0.2}V_{0.2}Nb_{0.2}Ta_{0.2})C$ and (right) the example multi-phase specimen of composition $(Zr_{0.2}Hf_{0.2}Ta_{0.2}Mo_{0.2}W_{0.2})C$.

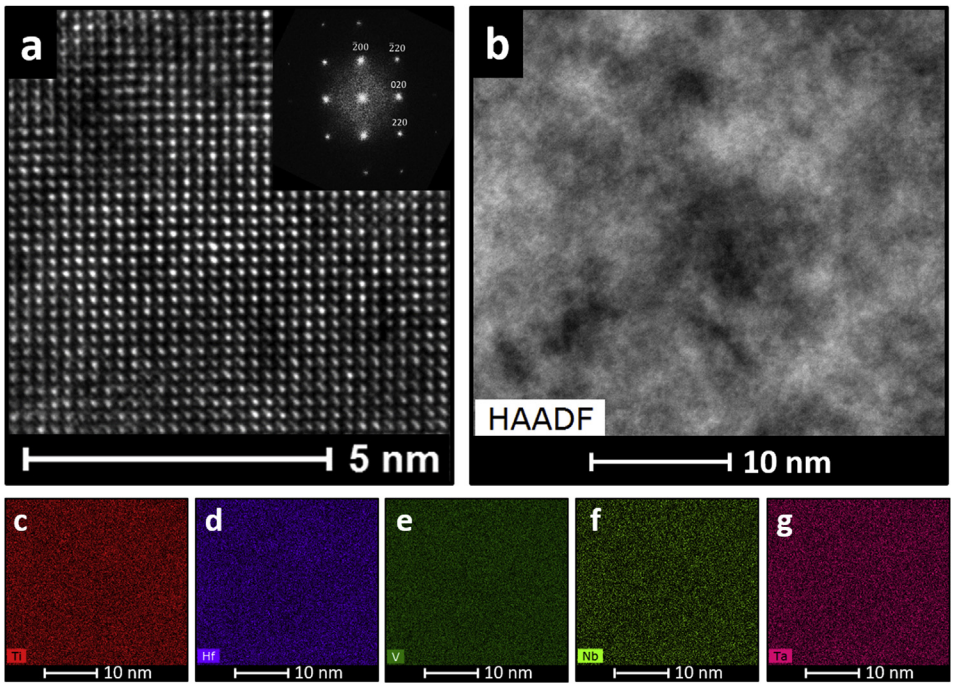

Fig. 4. (a) TEM and inset selected area electron diffraction (SAED) pattern, (b) STEM high angle annular dark field (HAADF) image and corresponding selected compositional maps from EDS for a sample of composition $(Ti_{0.2}Hf_{0.2}V_{0.2}Nb_{0.2}Ta_{0.2})C$. The SAED pattern is free of any additional points from secondary phases or long-range ordering. The compositional maps for (c) Ti, (d) Hf, (e) V, (f) Nb, and (g) Ta each appear homogeneous on the nanoscale and show no signs of chemical clustering.

the first nearest neighbor shell of each metal is carbon with a coordination number of six, and the second nearest neighbor shell is another metal atom with a coordination number of 12. The scattering paths in EXAFS have a degeneracy, D equal to the coordination number of that atom, therefore for a rocksalt carbide the single scattering path of the absorber to a metal in the second nearest neighbor shell would have a degeneracy of 12. For example, if one were to simulate a V-edge absorber within a vanadium monocarbide lattice, two single-scattering paths would be considered – first the single scattering event from the vanadium

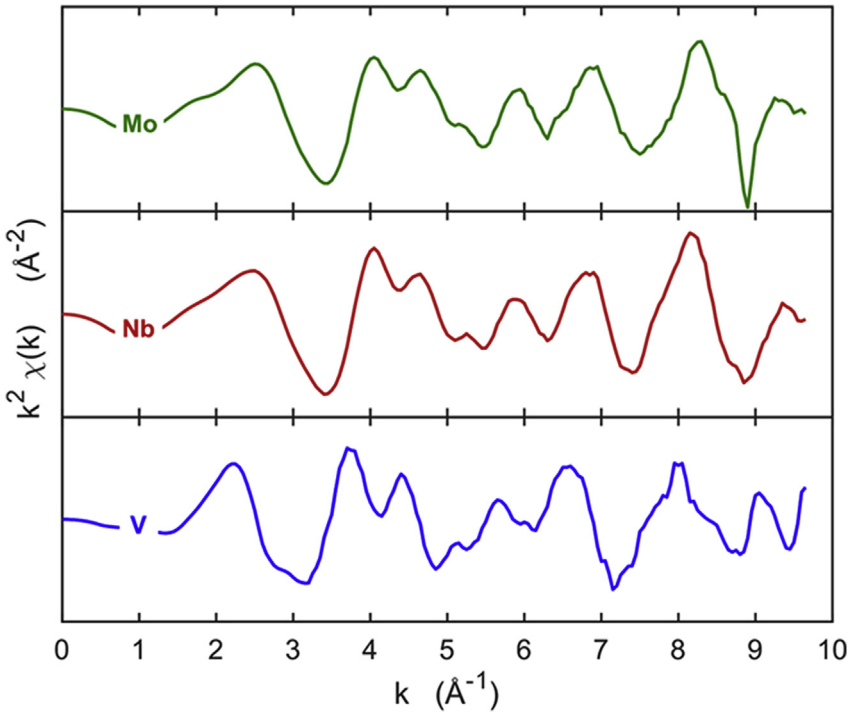

Fig. 5. XAFS for three of the metal absorbers in a sample of $(V_{0.2}Nb_{0.2}Ta_{0.2}Mo_{0.2}W_{0.2})C$, measured at the Advanced Photon Source beamline 12-BM after energy normalization and fitting. The oscillations appear at similar reciprocal spacings and with similar intensity.

absorber to the surrounding carbon atoms with a degeneracy of 6, then the single scattering path from the vanadium absorber to the second nearest neighbor vanadium with a degeneracy of 12. These two scattering paths would make up the majority of the signal for the first and second shells in the radial distribution function (RDF). By simulating a theoretical structure with the scattering path containing multiple different atoms and changing the degeneracy of each to fractions of the total degeneracy, partial occupancy can be represented. To do this, five separate single scattering paths from the vanadium absorber to the metal are added to the simulation. Geometrically they are all equivalent, however they assume that the metal atom is a different species. Each of the paths is weighted so that the total scattering path weight is $D = 12$ (i.e. $D_V = 2$, $D_{Nb} = 2.5$, $D_{Ta} = 2.5$, $D_{Mo} = 2.5$, $D_W = 2.5$). Each of the non-absorbing atoms are set to 2.5, while the absorber is set to 2 to simulate true mixing since the absorber would be surrounded by atoms other than itself. This is carried out with the results shown in Fig. 6, wherein the plots show the averaged experimental data from eight runs of the vanadium K-edge absorber in blue and the attempted fits to theoretical data in red. The second nearest neighbor shell was simulated as each of the elements, and then the mixed degeneracy from all five elements. The theoretical data is only shown to match the experimental data well when the metal shell is mixed occupancy and demonstrates significant error when it is modeled as any single metallic species.

3.5. Mechanical properties

The experimental elastic modulus and hardness results for five of the single-phase high entropy carbides are reported in Fig. 7 against their valence electron concentration (VEC) and rule of mixtures (RoM) expected values (tabulated values can be found in Supplementary Table 1). All HECs show significant hardness enhancements over the RoM predicted values. The hardness of transition metal carbides, nitrides and carbonitrides with the B1 structure is maximized when the VEC is equal to 8.4 [46–48]. An approximately monotonic correlation can be seen between the hardness and modulus and the VEC in the range from 8.4 to 9.4. As the VEC increases, the hardness decreases and the elastic modulus increases. A Pearson (linear) correlation coefficient of $r = -0.75$ and a Spearman's (rank) correlation coefficient of $\rho = -0.85$ demonstrate a negative correlation between hardness and VEC. Conversely, a Pearson correlation coefficient of $r = 0.78$ and Spearman's coefficient of $\rho = 0.65$ for modulus and VEC demonstrates a positive correlation. Supplementary Fig. 4 outlines a comparison of HECs in this study with the results of a comprehensive theoretical calculation from Ref. [48]. A comparison of strengthening and VEC is given in Supplementary Figure 5a where strengthening is defined as measured hardness minus the rule of mixtures predicted hardness. The results show that there is a correlation between the strengthening and the overall electronic structure of the final solid solution. Supplementary Figure 5b compares the strengthening to the carbon stoichiometry for four compositions, which demonstrates no noticeable relationship between the carbon content and the hardness increases.

4. Discussion

4.1. Phase formation

Given the list of compositions presented and the known solubilities of the group IVB, VB and VIB transition metal carbides, many of the compositions that exhibit single-phase materials are not surprising. It is well known that the group IVB and group VB carbides all exhibit extended mutual solid substitutional solubility [4]. It may be argued that mixing five B1 carbides that are all known to mix, amounts to no significant discovery when they are shown to do so. Hence, the compositions that contain only elements from

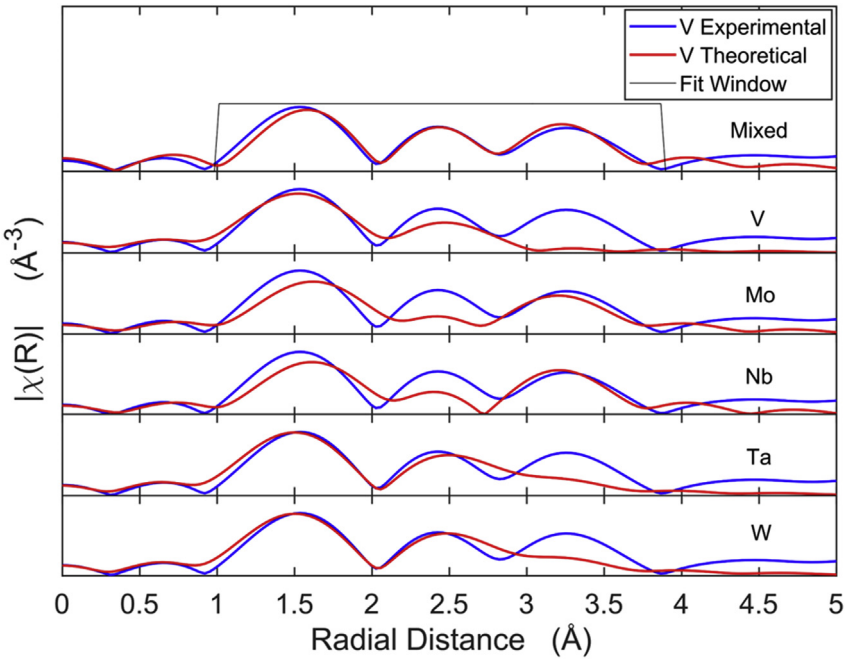

Fig. 6. Pseudo-radial distribution function from EXAFS measurements made on a vanadium absorber in a sample of composition $(V_{0.2}Nb_{0.2}Ta_{0.2}Mo_{0.2}W_{0.2})C$. The second nearest neighbor shell has a coordination number of 12, and therefore a degeneracy of 12 for the single scattering path. The theoretical fits (red) are attempted for the experimental data (blue) assuming the second nearest neighbor is a single metal species (W, Ta, Nb, Mo, V, from bottom to top) and then when the scattering path is weighted to be a combination of the five different metal species (mixed), which simulates a random distribution of nearest neighbors in the metal lattice. Note that the theoretical model only fits the data when the metal lattice is modeled as mixed and randomly oriented. (For interpretation of the references to colour in this figure legend, the reader is referred to the Web version of this article.)

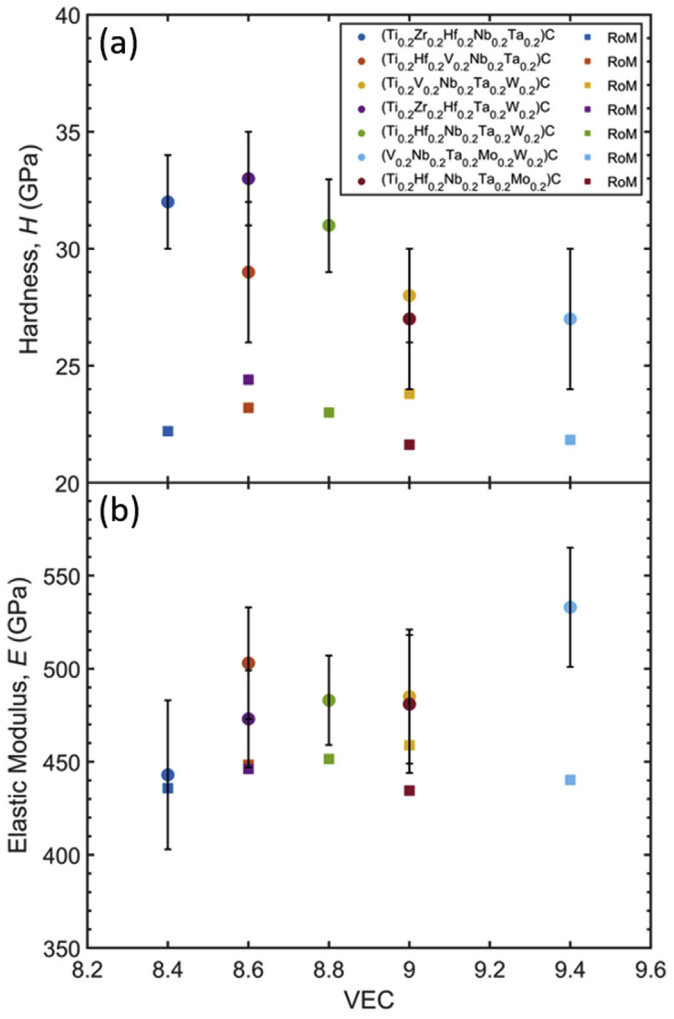

Fig. 7. (a) Hardness and (b) elastic moduli from nanoindentation (circle markers) on seven high entropy carbide compositions along with rule of mixture (RoM) values (square markers) against valence electron concentration (VEC). RoM values were calculated from experimental data in the current study and theoretical and experimental treatments in Refs. [41–44] for MoC and WC. Error bars are one standard deviation from 100 indents per sample.

group IVB and VB are likely enthalpically stable and are termed high entropy carbides, but not entropy stabilized carbides. However, the inclusion of the group VIB elements, which show limited solubility within the group IVB and VB metal carbides allows for a study of the effect of entropy in stabilizing the single phase. The EFA value for the composition $(V_{0.2}Nb_{0.2}Ta_{0.2}Mo_{0.2}W_{0.2})C$ is high indicating that the material should have a high entropic contribution and should easily form a single phase despite having both W and Mo. The inclusion of these two elements likely drives the system to instability on an enthalpic basis, so the formation of a single phase shows evidence for entropic stabilization. Experimental synthesis shows that $(V_{0.2}Nb_{0.2}Ta_{0.2}Mo_{0.2}W_{0.2})C$ does in fact easily form a random solid solution, providing evidence that the phase stability is a result of the high configurational entropy overcoming a positive enthalpy of formation, making this a true entropy stabilized material in the vein of the $(Co_{0.2}Cu_{0.2}Mg_{0.2}Ni_{0.2}Zn_{0.2})O$ oxide [16,45]. Further investigation of this composition is warranted and ongoing, including a so called "N-1" study, which involves removing a single element and determining if the four component systems maintain single phase stability, and calorimetry for determination of an endothermic phase transformation. As W and Mo are clearly the elements that drive up the enthalpy of formation of the rocksalt solid solution and destabilize it, it can be argued that the precursors used (hexagonal W_2C and orthorhombic Mo_2C) are more stable than their rocksalt analogues, and therefore would not undergo a phase transformation. This is likely not the case when considering the phases present in the final multi-phase specimens. The secondary and ternary phases are not the original hex-W_2C and Mo_2C that are present in the precursor. In two cases there are only cubic phases present, however these are in addition to the desired single rocksalt phase. This suggests that the thermodynamic equilibrium of the system at 2473 K (sintering temperature) consists of multiple phases rather than simply the W_2C and Mo_2C precursors remaining as remnant phases. The phase stability in each composition containing Mo and W is determined by the ability of the positive configurational entropy overcoming the positive enthalpy of formation of the solid solution. In $(V_{0.2}Nb_{0.2}Ta_{0.2}Mo_{0.2}W_{0.2})C$ the contribution is significant enough to overcome the enthalpy at 2473 K, where in $(Zr_{0.2}Hf_{0.2}Ta_{0.2}Mo_{0.2}W_{0.2})C$, $(Ti_{0.2}Zr_{0.2}Hf_{0.2}Mo_{0.2}W_{0.2})C$, and $(Zr_{0.2}Hf_{0.2}V_{0.2}Mo_{0.2}W_{0.2})C$ it is not. The final carbon stoichiometry for four of the compositions in Supplementary Table 2 are all within the range of 0.85 and 0.95, which suggests that the carbon content is not heavily dependent on the initial carbon content of the precursors, but in a carbon rich sintering environment above 2273 K each of the compositions approaches an equilibrium stability. This is not surprising when considering the maximum stability of carbides falls at a VEC of 8.4, so each sample will approach a certain substoichiometry that moves the overall composition closer to this value [46–48].

4.2. Mechanical properties

The hardness enhancement in high entropy carbides has been reported in the preliminary works by the present authors [28,31], Castle et al. [29], and Yan et al., [32]. Solid solution strengthening undoubtedly has an effect on the mechanical performance of the alloys, however certain alloys display significant enhancements over the rule of mixtures predicted values, which cannot be fully explained by traditional solid solution strengthening mechanisms (i.e. dislocation inhibition by solute atoms). The complex nature of the d-orbital bonding in the transition metal nitrides and carbides is still not fundamentally well understood, which makes a true calculation of solid solution strengthening effects unattainable [49]. It has even been suggested in transition metal carbides and nitrides with the B1 structure, that the mechanical properties, such as hardness, depend more significantly on the nature of the bonding than on the microstructural features [3,46–48]. This implies that the hardness of the solid solution of five transition metal carbides will likely demonstrate dependence both on the mechanical properties of the individual constituents within the solid solution, and on the overall electronic structure of the final phase. Hence, a comparison of the hardness and modulus of each of the carbides to the VEC can reveal the contribution of the electronic mechanism behind the hardness enhancements. The results show agreement with the *ab initio* study in Ref. [48], that the hardness of carbides decreases as a function of VEC from 8.4 to 9.4. The modulus of the HECs is shown to increase with VEC, which is seemingly in contrast to what is normally reported, however the comparison to the modulus data (Supplementary Fig. 4) shows that the modulus of the ternary nitrides and carbonitrides increases for most materials up to a maximum near VEC 9 then decreases to a VEC of 11. Further characterization of HECs with VEC greater than 9.4 (the maximum in this study) could determine whether the modulus begins to decrease. It has also been shown both experimentally and through theoretical investigations that the toughness of B1 structured transition metal carbides and nitrides increases with increasing VEC [50,51]. This is

demonstrated in studies that explore the different deformation mechanisms that lead to the mechanical properties of HfC and TaC. HfC and TaC are similarly structured and bonded ceramics, yet TaC shows significant plasticity and dislocation formation and motion when deformed at room temperature, while HfC shows very little plasticity by comparison [52,53]. The work of De Leon et al. in Ref. [53] attributes this to the difference in electronic structure that leads to an intrinsic stacking fault in TaC, which promotes dissociation of dislocations into partials on the {111} and causes the dominant slip system to be the a/2<110>{111}, while in HfC the a/2<110>{110} system is dominant. The work of Castle et al. [29] agrees that comparison of the hardness of four component solid solution carbides to the rule of mixtures average of the binary constituents is not warranted, as different electronic structures lead to different slip conditions. The experimental results across the five component compositions in this study reveal that the high entropy carbides do show a general trend of decreasing hardness and increasing modulus with increasing VEC, however there also exists significant deviations amongst multiple systems with the same VEC. For instance, the compositions $(Ti_{0.2}Hf_{0.2}V_{0.2}Nb_{0.2}Ta_{0.2})C$ and $(Ti_{0.2}Zr_{0.2}Hf_{0.2}Ta_{0.2}W_{0.2})C$ each have a VEC of 8.6, while their hardness values are 29 GPa and 33 GPa, respectively. This suggests that the deformation mechanisms and, therefore, mechanical properties are at least partially dependent on the electronic structure, but the VEC parameter may be an oversimplification of the electronic density of states, which depends on the structure and bonding characteristics of each of the constituent elements and carbon. Further, as also suggested by Castle et al. [29], traditional solid solution strengthening likely does have an effect on the overall hardness measured in high entropy carbides and an analysis of trends over a range of VECs as well as trends over a range of compositions with the same VEC can allow for isolation of hardness increases from solid solution effects and hardness increases from electronic effects. Although a clear model for solid solution strengthening is a difficult task in HECs, since they are all five-component, equiatomic solid solutions we can justify that they would all show similar strengthening over the rule of mixtures average of the binaries regardless of the electronic structure. When comparing strengthening to VEC (Supplementary Figure 5a), however, there is a clear relationship, which reinforces that there is more than just solid solution strengthening effects and that different solutions exhibit different deformation mechanics that are dependent on the average electronic structure of the solid solution. Clearly, further work regarding the complete electronic density of states of each complex composition and its relationship to the deformation mechanisms is warranted and ongoing. The dependence of the mechanical properties on the electronic state of the material, however, gives a route to further tunability of mechanical properties of carbides and the exploration of the high entropy composition space gives access to a new library of electronic states that may be inaccessible via simply binary and ternary carbides.

5. Conclusion

This study explores phase formation in twelve different five-metal high entropy carbide ceramic compositions. Nine of the twelve compositions are determined to be single-phase solid solutions when sintered at 2473 K. We conclude that:

- These materials represent an exploration of a new composition space in ceramics that may lead to improved UHTCs.
- Addition of tungsten and molybdenum into systems with three group IVB or VB transition metals lowers the chance of forming a single phase, however systems can be synthesized that form a single phase with both Mo and W.
- The phase stability depends on a trade-off between enthalpy and entropy, and we find evidence for entropic stabilization (rather than simply high entropy) in the composition $(V_{0.2}Nb_{0.2}Ta_{0.2}Mo_{0.2}W_{0.2})C$, which warrants further investigation.
- Single-phase materials were homogeneous on multiple length scales from characterization in XRD, SEM-EDS, S/TEM-EDS, and EXAFS analysis.
- The high entropy transition metal carbides show significantly enhanced hardness over the weighted average of the binary constituents. Comparison to the average of the binary constituent carbides is ineffective in predicting hardness enhancements.
- The mechanical properties follow theories of electronic structure mechanisms in carbides and nitrides, and support trends of hardness decreasing with increasing valence electron concentration.
- Evidence shows that enhanced mechanical properties are not dependent on entropic stabilization and can be exploited as long as the material is randomly mixed (a true high entropy) material (i.e. they must be high entropy rather than just multicomponent, but do not necessarily need to be entropy stabilized). However, the discovery of entropically-stabilized phases may lead to enhanced properties previously unattainable at high temperatures.

Acknowledgements

The authors acknowledge support through the Office of Naval Research ONR-MURI (grant No. N00014-15-1-2863). This research used resources of the Advanced Photon Source, a U.S. Department of Energy (DOE) Office of Science User Facility operated for the DOE Office of Science by Argonne National Laboratory under Contract No. DE-AC02-06CH11357. K. Kaufmann was supported by the Department of Defense through the National Defense Science & Engineering Graduate Fellowship (NDSEG) Program. K. Kaufmann would also like to acknowledge the generous support of the ARCS Foundation, San Diego Chapter. The authors thank APS BM-12B beamline scientist Dr. Benjamin Reinhart for aid in EXAFS data collection, and Lavina Backman, Jeffrey Braun, Trent Borman, Dr. Jon-Paul Maria and Dr. Elizabeth Opila for guidance and helpful scientific discussion.

Appendix A. Supplementary data

Supplementary data to this article can be found online at https://doi.org/10.1016/j.actamat.2018.12.054.

References

[1] E. Wuchina, E. Opila, M. Opeka, W. Fahrenholtz, I. Talmy, UHTCs: ultra-high temperature ceramics for extreme environment applications, Electrochem. Soc. Interface. 16 (2007) 30.
[2] O. Cedillos-Barraza, D. Manara, K. Boboridis, T. Watkins, S. Grasso, D.D. Jayaseelan, R.J.M. Konings, M.J. Reece, W.E. Lee, Investigating the highest melting temperature materials: a laser melting study of the TaC-HfC system, Sci. Rep. 6 (2016) 37962, https://doi.org/10.1038/srep37962.
[3] L. Toth, Transition Metal Carbides and Nitrides, Academic Press, Inc., New York, 1971.
[4] H.O. Pierson, Handbook of Refractory Carbides and Nitrides : Properties, Characteristics, Processing, and Applications, Noyes Publications, New Jersey, USA, 1996.
[5] B.S. Murty, Jien-Wei Yeh, S. Ranganathan, High-entropy Alloys, Butterworth-Heinemann, London, UK, 2014.
[6] M.-H. Tsai, J.-W. Yeh, High-entropy alloys: a critical review, Mater. Res. Lett. 2 (2014) 107–123, https://doi.org/10.1080/21663831.2014.912690.
[7] D.B. Miracle, O.N. Senkov, A critical review of high entropy alloys and related concepts, Acta Mater. 122 (2017) 448–511, https://doi.org/10.1016/J.ACTAMAT.2016.08.081.

[8] D.B. Miracle, Critical Assessment 14: high entropy alloys and their development as structural materials, Mater. Sci. Technol. 31 (2015) 1142–1147, https://doi.org/10.1179/1743284714Y.0000000749.
[9] F. Otto, Y. Yang, H. Bei, E.P. George, Relative effects of enthalpy and entropy on the phase stability of equiatomic high-entropy alloys, Acta Mater. 61 (2013) 2628–2638, https://doi.org/10.1016/J.ACTAMAT.2013.01.042.
[10] Y. Zhang, T.T. Zuo, Z. Tang, M.C. Gao, K.A. Dahmen, P.K. Liaw, Z.P. Lu, Microstructures and properties of high-entropy alloys, Prog. Mater. Sci. 61 (2014) 1–93, https://doi.org/10.1016/J.PMATSCI.2013.10.001.
[11] É. Fazakas, V. Zadorozhnyy, L.K. Varga, A. Inoue, D.V. Louzguine-Luzgin, F. Tian, L. Vitos, Experimental and theoretical study of Ti20Zr20Hf20Nb20X20 (X=V or Cr) refractory high-entropy alloys, Int. J. Refract. Metals Hard Mater. 47 (2014) 131–138, https://doi.org/10.1016/j.ijrmhm.2014.07.009.
[12] O.N. Senkov, G.B. Wilks, D.B. Miracle, C.P. Chuang, P.K. Liaw, Refractory high-entropy alloys, Intermetallics 18 (2010) 1758–1765, https://doi.org/10.1016/J.INTERMET.2010.05.014.
[13] A. Poulia, E. Georgatis, A. Lekatou, A.E. Karantzalis, Microstructure and wear behavior of a refractory high entropy alloy, Int. J. Refract. Metals Hard Mater. 57 (2016) 50–63, https://doi.org/10.1016/J.IJRMHM.2016.02.006.
[14] O.N. Senkov, G.B. Wilks, J.M. Scott, D.B. Miracle, Mechanical properties of Nb25Mo25Ta25W25 and V20Nb20Mo20Ta20W20 refractory high entropy alloys, Intermetallics 19 (2011) 698–706, https://doi.org/10.1016/J.INTERMET.2011.01.004.
[15] J. Gild, M. Samiee, J.L. Braun, T. Harrington, H. Vega, P.E. Hopkins, K. Vecchio, J. Luo, High-entropy fluorite oxides, J. Eur. Ceram. Soc. 38 (2018) 3578–3584, https://doi.org/10.1016/J.JEURCERAMSOC.2018.04.010.
[16] C.M. Rost, E. Sachet, T. Borman, A. Moballegh, E.C. Dickey, D. Hou, J.L. Jones, S. Curtarolo, J.-P. Maria, Entropy-stabilized oxides, Nat. Commun. 6 (2015) 8485, https://doi.org/10.1038/ncomms9485.
[17] D. Bérardan, S. Franger, A.K. Meena, N. Dragoe, Room temperature lithium superionic conductivity in high entropy oxides, J. Mater. Chem. A. 4 (2016) 9536–9541, https://doi.org/10.1039/C6TA03249D.
[18] D. Bérardan, S. Franger, D. Dragoe, A.K. Meena, N. Dragoe, Colossal dielectric constant in high entropy oxides, Phys. Status Solidi Rapid Res. Lett. 10 (2016) 328–333, https://doi.org/10.1002/pssr.201600043.
[19] D.B. Miracle, High-entropy alloys: a current evaluation of founding ideas and core effects and exploring “nonlinear alloys, JOM (J. Occup. Med.) 69 (2017) 2130–2136, https://doi.org/10.1007/s11837-017-2527-z.
[20] J. Gild, Y. Zhang, T. Harrington, S. Jiang, T. Hu, M.C. Quinn, W.M. Mellor, N. Zhou, K. Vecchio, J. Luo, High-entropy metal diborides: a new class of high-entropy materials and a new type of ultrahigh temperature ceramics, Sci. Rep. 6 (2016) 37946, https://doi.org/10.1038/srep37946.
[21] C.-H. Lai, S.-J. Lin, J.-W. Yeh, S.-Y. Chang, Preparation and characterization of AlCrTaTiZr multi-element nitride coatings, Surf. Coating. Technol. 201 (2006) 3275–3280, https://doi.org/10.1016/j.surfcoat.2006.06.048.
[22] T.K. Chen, T.T. Shun, J.W. Yeh, M.S. Wong, Nanostructured nitride films of multi-element high-entropy alloys by reactive DC sputtering, Surf. Coating. Technol. 188–189 (2004) 193–200, https://doi.org/10.1016/j.surfcoat.2004.08.023.
[23] T.-T. Shun, Y.-C. Du, Age hardening of the Al0.3CoCrFeNiC0.1 high entropy alloy, J. Alloy. Comp. 478 (2009) 269–272, https://doi.org/10.1016/j.jallcom.2008.12.014.
[24] H. Fager, J.M. Andersson, J. Jensen, J. Lu, L. Hultman, Thermal stability and mechanical properties of amorphous coatings in the Ti-B-Si-Al-N system grown by cathodic arc evaporation from TiB_2, $Ti_{33}Al_{67}$, and $Ti_{85}Si_{15}$ cathodes, J. Vac. Sci. Technol. A Vacuum, Surfaces, Film. 32 (2014), 061508, https://doi.org/10.1116/1.4897170.
[25] V.F. Gorban, A.A. Andreyev, G.N. Kartmazov, A.M. Chikryzhov, M.V. Karpets, A.V. Dolomanov, A.A. Ostroverkh, E.V. Kantsyr, Production and mechanical properties of high-entropic carbide based on the TiZrHfVNbTa multicomponent alloy, J. Superhard Mater. 39 (2017) 166–171, https://doi.org/10.3103/S1063457617030030.
[26] A. Vladescu, I. Titorencu, Y. Dekhtyar, V. Jinga, V. Pruna, M. Balaceanu, M. Dinu, I. Pana, V. Vendina, M. Braic, In vitro biocompatibility of Si alloyed multi-principal element carbide coatings, PLoS One 11 (2016), e0161151, https://doi.org/10.1371/journal.pone.0161151.
[27] V. Braic, A. Vladescu, M. Balaceanu, C.R. Luculescu, M. Braic, Nanostructured multi-element (TiZrNbHfTa)N and (TiZrNbHfTa)C hard coatings, Surf. Coating. Technol. 211 (2012) 117–121, https://doi.org/10.1016/J.SURFCOAT.2011.09.033.
[28] P. Sarker, T. Harrington, C. Toher, C. Oses, M. Samiee, J.-P. Maria, D.W. Brenner, K.S. Vecchio, S. Curtarolo, High-entropy high-hardness metal carbides discovered by entropy descriptors, Nat. Commun. 9 (2018) 4980, https://doi.org/10.1038/s41467-018-07160-7.
[29] E. Castle, T. Csanádi, S. Grasso, J. Dusza, M. Reece, Processing and properties of high-entropy ultra-high temperature carbides, Sci. Rep. 8 (2018) 8609, https://doi.org/10.1038/s41598-018-26827-1.
[30] J. Dusza, P. Švec, V. Girman, R. Sedlák, E.G. Castle, T. Csanádi, A. Kovalčíková, M.J. Reece, Microstructure of (Hf-Ta-Zr-Nb)C high-entropy carbide at micro and nano/atomic level, J. Eur. Ceram. Soc. 38 (2018) 4303–4307, https://doi.org/10.1016/J.JEURCERAMSOC.2018.05.006.
[31] Kenneth Vecchio, Jian Luo, Joshua Gild, Mojtaba Samiee, Olivia F. Dippo, Tyler J. Harrington, Stefano Curtarolo, Pranab Sarker, Cormac Toher, Modelling and synthesis of high-entropy refractory carbides, nitrides and carbonitrides, in: Jon Binner (Ed.), Ultra-high Temperature Ceramics: Materials for Extreme Environment Applications IV, The University of Birmingham, Edgbaston, United Kingdom Bill Lee, Imperial College, London, United Kingdom, 2017. ECI Symposium Series, http://dc.engconfintl.org/uhtc_iv/32.
[32] X. Yan, L. Constantin, Y. Lu, J.-F. Silvain, M. Nastasi, B. Cui, $(Hf_{0.2}Zr_{0.2}Ta_{0.2}Nb_{0.2}Ti_{0.2})C$ high-entropy ceramics with low thermal conductivity, J. Am. Ceram. Soc. 101 (2018) 4486–4491, https://doi.org/10.1111/jace.15779.
[33] K. Yang, C. Oses, S. Curtarolo, Modeling off-stoichiometry materials with a high-throughput ab-initio approach, Chem. Mater. 28 (2016) 6484–6492, https://doi.org/10.1021/acs.chemmater.6b01449.
[34] S. Curtarolo, W. Setyawan, G.L.W. Hart, M. Jahnatek, R.V. Chepulskii, R.H. Taylor, S. Wang, J. Xue, K. Yang, O. Levy, M.J. Mehl, H.T. Stokes, D.O. Demchenko, D. Morgan, AFLOW: an automatic framework for high-throughput materials discovery, Comput. Mater. Sci. 58 (2012) 218–226, https://doi.org/10.1016/J.COMMATSCI.2012.02.005.
[35] G. Kresse, J. Furthmüller, Efficient iterative schemes for *ab initio* total-energy calculations using a plane-wave basis set, Phys. Rev. B 54 (1996) 11169–11186, https://doi.org/10.1103/PhysRevB.54.11169.
[36] J.P. Perdew, K. Burke, M. Ernzerhof, Generalized gradient approximation made simple, Phys. Rev. Lett. 77 (1996) 3865–3868, https://doi.org/10.1103/PhysRevLett.77.3865.
[37] C.E. Calderon, J.J. Plata, C. Toher, C. Oses, O. Levy, M. Fornari, A. Natan, M.J. Mehl, G. Hart, M. Buongiorno Nardelli, S. Curtarolo, The AFLOW standard for high-throughput materials science calculations, Comput. Mater. Sci. 108 (2015) 233–238, https://doi.org/10.1016/J.COMMATSCI.2015.07.019.
[38] B. Ravel, M. Newville, ATHENA, ARTEMIS, HEPHAESTUS: data analysis for X-ray absorption spectroscopy using IFEFFIT, J. Synchrotron Radiat. 12 (2005) 537–541.
[39] A. Nino, A. Tanaka, S. Sugiyama, H. Taimatsu, Indentation size effect for the hardness of refractory carbides, Mater. Trans. 51 (2010) 1621–1626, https://doi.org/10.2320/matertrans.M2010110.
[40] W.C. Oliver, G.M. Pharr, An improved technique for determining hardness and elastic modulus using load and displacement sensing indentation experiments, J. Mater. Res. 7 (1992) 1564–1583, https://doi.org/10.1557/JMR.1992.1564.
[41] Y. Liu, Y. Jiang, J. Feng, R. Zhou, Elasticity, electronic properties and hardness of MoC investigated by first principles calculations, Phys. B Condens. Matter 419 (2013) 45–50, https://doi.org/10.1016/J.PHYSB.2013.03.016.
[42] D.V. Suetin, I.R. Shein, A.L. Ivanovskii, Elastic and electronic properties of hexagonal and cubic polymorphs of tungsten monocarbide WC and mononitride WN from first-principles calculations, Phys. Status Solidi 245 (2008) 1590–1597, https://doi.org/10.1002/pssb.200844077.
[43] A.A. Voevodin, J.P. O'Neill, S.V. Prasad, J.S. Zabinski, Nanocrystalline WC and WC/a-C composite coatings produced from intersected plasma fluxes at low deposition temperatures, J. Vac. Sci. Technol. A Vacuum, Surfaces, Film. 17 (1999) 986, https://doi.org/10.1116/1.581674.
[44] Y. Pauleau, P. Gouy-Pailler, Characterization of tungsten-carbon layers deposited on stainless steel by reactive magnetron sputtering, J. Mater. Res. 7 (1992) 2070–2079, https://doi.org/10.1557/JMR.1992.2070.
[45] C. Rost, Entropy-stabilized oxides: Explorations of a Novel class of Multi-component Materials, PhD Dissertation, NCSU, 2016, http://www.lib.ncsu.edu/resolver/1840.16/11411.
[46] S.-H. Jhi, J. Ihm, S.G. Louie, M.L. Cohen, Electronic mechanism of hardness enhancement in transition-metal carbonitrides, Nature 399 (1999) 132–134, https://doi.org/10.1038/20148.
[47] V. Richter, A. Beger, J. Drobniewski, I. Endler, E. Wolf, Characterisation and wear behaviour of TiN- and TiCxN1-x-coated cermets, Mater. Sci. Eng. 209 (1996) 353–357, https://doi.org/10.1016/0921-5093(95)10109-8.
[48] K. Balasubramanian, S.V. Khare, D. Gall, Valence electron concentration as an indicator for mechanical properties in rocksalt structure nitrides, carbides and carbonitrides, Acta Mater. 152 (2018) 175–185, https://doi.org/10.1016/J.ACTAMAT.2018.04.033.
[49] F. Gao, Hardness of cubic solid solutions, Sci. Rep. 7 (2017) 40276, https://doi.org/10.1038/srep40276.
[50] D.G. Sangiovanni, V. Chirita, L. Hultman, Electronic mechanism for toughness enhancement in Ti x M 1 − x N (M = Mo and W), Phys. Rev. B 81 (2010) 104107, https://doi.org/10.1103/PhysRevB.81.104107.
[51] D.G. Sangiovanni, L. Hultman, V. Chirita, Supertoughening in B1 transition metal nitride alloys by increased valence electron concentration, Acta Mater. 59 (2011) 2121–2134, https://doi.org/10.1016/J.ACTAMAT.2010.12.013.
[52] N. De Leon, X. Yu, H. Yu, C.R. Weinberger, G.B. Thompson, Bonding effects on the slip differences in the B 1 monocarbides, Phys. Rev. Lett. 114 (2015) 165502, https://doi.org/10.1103/PhysRevLett.114.165502.
[53] S. Kiani, J.-M. Yang, S. Kodambaka, Nanomechanics of refractory transition-metal carbides: a path to discovering plasticity in hard ceramics, J. Am. Ceram. Soc. 98 (2015) 2313–2323, https://doi.org/10.1111/jace.13686.